Determination of the absolute chirality of tellurium using resonant diffraction with circularly polarized x-rays

2010 J. Phys.: Condens. Matter 22 122201

(http://iopscience.iop.org/0953-8984/22/12/122201)

IOP FTC
IOP Publishing
Journal of Physics: Condensed Matter
J. Phys.: Condens. Matter **22** (2010) 122201 (7pp)
doi:10.1088/0953-8984/22/12/122201

FAST TRACK COMMUNICATION

Determination of the absolute chirality of tellurium using resonant diffraction with circularly polarized x-rays

Y Tanaka[1], S P Collins[2], S W Lovesey[3], M Matsumami[1], T Moriwaki[4] and S Shin[1]

[1] RIKEN SPring-8 Centre, Sayo, Hyogo 679-5148, Japan
[2] Diamond Light Source Ltd, Diamond House, Harwell Science and Innovation Campus, Didcot, Oxfordshire OX11 0DE, UK
[3] ISIS Facility and Diamond Light Source, Rutherford Appleton Laboratory, Oxfordshire OX11 0QX, UK
[4] Japan Synchrotron Radiation Research Institute (JASRI), Sayo, Hyogo 679-5198, Japan

E-mail: ytanaka@riken.jp

Received 17 December 2009, in final form 15 February 2010
Published 8 March 2010
Online at stacks.iop.org/JPhysCM/22/122201

Abstract
Many proteins, sugars and pharmaceuticals crystallize into two forms that are mirror images of each other (enantiomers) like our right and left hands. Tellurium is one enantiomer having a space group pair, $P3_121$ (right-handed screw) and $P3_221$ (left-handed screw). X-ray diffraction with dispersion correction terms has been playing an important role in determining the handedness of enantiomers for a long time. However, this approach is not applicable for an elemental crystal such as tellurium or selenium. We have demonstrated that positive and negative circularly polarized x-rays at the resonant energy of tellurium can be used to absolutely distinguish *right* from *left* tellurium. This method is applicable to chiral motifs that occur in biomolecules, liquid crystals, ferroelectrics and antiferroelectrics, multiferroics, etc.

(Some figures in this article are in colour only in the electronic version)

1. Introduction

It is well known that there are two kinds of crystal structure for low quartz and that visible light passing through a crystal rotates the polarization plane clockwise or counterclockwise according to the crystal structure. This phenomenon, optical activity, can be found in natural organic substances such as sugar, camphor or tartaric acid as well as in inorganic materials like tellurium. Many of these molecules or crystals have enantiomers, or stereoisomers whose atomic configurations are mirror images of each other and are thus handed, like our right and left hands. This geometrical property of crystals and molecules is called as chirality.

Determination of the absolute structure has been one of the important issues of crystallography. Among several methods developed for the determination so far, x-ray diffraction with the dispersion correction has been playing an important role for a long time. The scattering length of x-rays for an atom can be written as

$$f = f_0 + f' + \mathrm{i}f'', \tag{1}$$

where f_0 is the energy-independent x-ray scattering length and the Fourier transform of the electron density around the atom, f' and f'' are the real and the imaginary parts of the dispersion correction, respectively. It has been known that these correction terms depend on the wavelength or the energy of x-ray beam and that the effect is significant at the absorption edge of the resonant element. The term f'', which plays an important role and has a negative value corresponding to the expression of phase $\exp \mathrm{i}(kz - \omega t)$ for a plane wave, has the minimum at the absorption edge of the resonant element, and

some amount at the higher energies. Here the plane wave propagates along the positive z direction with a wavenumber $k > 0$ and an angular frequency $\omega > 0$.

The method was first applied to solve the absolute configuration of tartaric acid and carbohydrates by Bijvoet *et al* in 1951 [1], and has since been developed extensively and applied to the determination of the absolute configuration of numerous biochemical compounds. For example the multi-wavelength anomalous diffraction (MAD) has been developed to determine the atomic configuration of complex macromolecular systems in biology [2].

This method, however, is not applicable to determining the chiral structure of an elemental material like selenium or tellurium. In general, the unit-cell structure factor is given as $F = F' + \mathrm{i}F''$, and F' and F'' are the real and the imaginary parts, respectively. The method described above uses the fact that the ratio F''/F' changes as a function of the energy because the structure factor is a sum of the scattering lengths of non-resonant atoms and those of resonant atoms of which f'' significantly changes around the absorption edge. Therefore the ratio of intensity of reflections for different Miller indices hkl changes as a function of the energy. However, for an elemental material, all the scattering length are uniformly multiplied by the f'' and, accordingly, the ratio of intensity of reflections for any Miller indices are independent of the energy.

In the literature, some techniques have been proposed for the determination of the chiral structure of tellurium using dispersion corrections [3, 4], however, no successful experimental evidence has been so far reported to the best of our knowledge. As far as we are aware, the only successful measurement is the work of Brown *et al*, who determined the chirality of tellurium using polarized neutron diffraction, utilizing the polarization dependence of Schwinger scattering [5]. They have found that the tellurium crystal which shows laevorotatory optical rotatory power (the polarization plane of the light rotates to the counterclockwise direction as seen by an observer looking through the crystal towards the light source) belongs to the space group $P3_121$ (#152 right-handed) but not to the space group $P3_221$ (#154 left-handed).

Our method is quite different from the x-ray and neutron diffraction techniques described above. We use resonant x-ray diffraction for which the x-ray energy is close to an atomic absorption edge, where the x-ray dichroism and the x-ray scattering strongly depend on the *polarization* state of x-rays. This property was demonstrated by Templeton and Templeton in 1980 [6] and in 1982 [7]. Dmitrienko *et al* introduced the anisotropy of x-ray susceptibility to describe the resonant x-ray diffraction for non-magnetic materials, and summarized in a recent review [8]. Lovesey *et al* formulated the resonant x-ray diffraction for non-magnetic and magnetic media by introducing the atomic tensor [9].

The crystal structure of tellurium is described by an enantiomorphic space group pair, namely, $P3_121$ (#152) and $P3_221$ (#154). Accordingly, it has handedness. Hereafter we describe tellurium which belongs to $P3_121$ as R Te (right screw) and tellurium which belongs to $P3_221$ as L Te (left screw) according to their screw structures in the space groups. Figure 1 shows the structure of R Te and L Te. The unit-cell

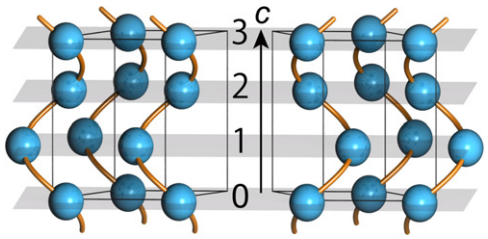

Figure 1. Structure of Te for space group #152 (right) and space group #154 (left). Blue spheres represent Te atoms. Black lines show the unit cell for each crystal. Screw lines for each panel are a guide to eyes. An arrow shows the c axis of these structure.

parameters of tellurium at 300 K are $a = 4.46$ Å, $c = 5.93$ Å. In space group $P3_121$ (R Te), the atomic position Te is at $3a$ (x, 0, $\frac{1}{3}$) with $x = 0.263$ [10]. There are three Te atoms in a unit cell. The difference between space group $P3_121$ and $P3_221$ is simply on the stacking sequence of atomic planes along the c axis. The sequence for each space group is in the opposite direction.

In conventional x-ray diffraction, none of the terms in equation (1) depends on the polarization state of x-ray beam. Therefore the scattering length of Te atoms in plane 0 is equivalent to those of plane 1 and plane 2 and the minimum unit for reflection $00l$ is $\frac{c}{3}$. Thus, $00l$, $l = 3n$ (n is an integer), is observed and reflection 001 is forbidden because there are two planes between plane 0 and plane 3 and the unit-cell structure factor is cancelled out by taking a sum. However, the resonant x-ray diffraction in the vicinity of the absorption edge of the target element depends strongly on the *polarization* state of x-rays. Therefore the scattering length of Te atoms in plane 0 is not equivalent to those of plane 1 and plane 2 any more. In this case, the minimum unit for reflection $00l$ is c, thus reflection 001 is observable.

The relations between the optical activity and the crystal structure for many materials has been intensively discussed by Glazer *et al* [11]. Nomura has reported that tellurium shows a strong optical dextro (right)- and laevo (left)-rotatory power for the infrared radiation [12]. However, the relationship between the sense of rotatory power and the structural chirality had been unknown until the neutron diffraction work [5].

We have shown that circularly polarized x-rays differentiate the crystal chirality by coupling to the crystal screw axis in low quartz [13, 14]. However, the results are not sufficient to determine the structural chirality by themselves because the mixture of two resonant processes gives a complicated theoretical formula and prevents us from determining the sign of chirality. Here we use the term 'structural chirality' and concern ourselves with the sign of chirality in spaces group which have the screw axes labelled right-handed (3_1, 4_1, 6_1, 6_2) and left-handed (3_2, 4_3, 6_5, 6_4). We aim to distinguish one handedness from its inverse for a single crystal for which the handedness is unknown.

In the present paper, we demonstrate that circularly polarized x-rays provides a sufficient and elegant tool to determine the sign of chirality of crystals absolutely with the resonance effect described only by the $E1E1$ process. Here we

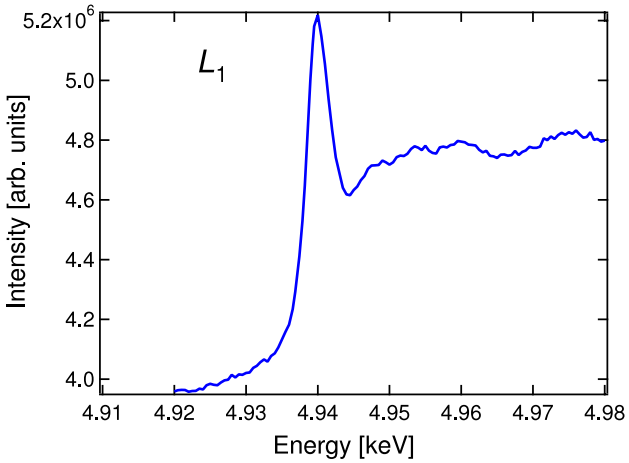

Figure 2. XAS obtained by the total fluorescence yield in the vicinity of Te L_1 absorption edge.

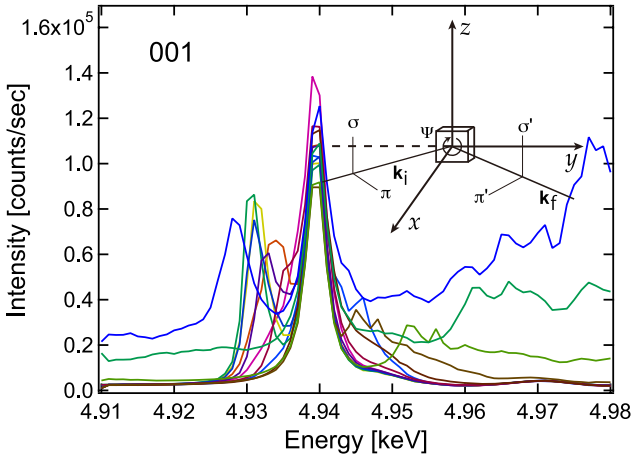

Figure 3. Energy spectra of forbidden reflection 001 around L_1 as a function of energy and azimuth angle Ψ. Each line shows an energy spectrum for an azimuth angle Ψ which is scanned in a range from $\Psi = -56.45$ to -69.2. Lines are drawn with every two steps of Ψ to simplify the figure. Inset shows a schematic view of Bragg diffraction with a right-handed coordinates x, y, and z.

present the results of resonant x-ray diffraction on tellurium crystal and show that they give unambiguous evidence to determine the structural chirality.

2. Experiment and results

The experiment has been carried out on the beamline I16 at the Diamond Light Source, UK. The tellurium sample, cut to 5 mm × 4 mm × 5 mm in size was mounted on a Kappa diffractometer. The surface of the sample was normal to the c axis. The chirality of the sample was unknown. First we determined the a^* axis, measuring the intensity of six reflections 101, 011, $\bar{1}11$, $\bar{1}01$, $0\bar{1}1$, and $1\bar{1}1$. In principle we cannot fix the a^* axis as we do not know the space group. The reason is as follows. Each of these six reflections has the same Bragg angle, but the intensity is not equivalent. Among them, three reflections 101, $\bar{1}11$, $0\bar{1}1$ are stronger, and the others are weaker for R Te, however, this relation of intensity is opposite for L Te. As we show later, our sample is R Te. Here for convenience we suppose that the sample is R Te and we fix the axes a, b, and c by choosing one of three stronger reflections among the six reflections and defining the Miller index of the reflection for example as 101. This definition does not depend on the determination of the chirality, of course.

2.1. Energy scans

Figure 2 shows the x-ray absorption spectrum (XAS) obtained in the total x-ray fluorescence yield mode in the vicinity of the Te L_1 absorption edge. We have measured XAS in the vicinity of Te L_2 and L_3 absorption edges (not shown), however, only XAS at the L_1 absorption edge shows a sharp peak. This is because the 4d band in tellurium is fully filled and the resonant 2p ↔ 4d is suppressed while the 5p band is not fully filled and the resonant 2s ↔ 5p is allowed.

The general diffraction geometry is illustrated in the inset of figure 3. The scattering plane is spanned by vectors $\mathbf{k}_i$ and $\mathbf{k}_f$, which are the propagation vectors of the incident and diffracted beams, respectively. The σ and σ' are linear components of x-rays perpendicular to the scattering plane for the incident and diffracted beam, respectively (parallel to the z axis), and their Stoke parameters [15, 16], which represents the polarization of the x-ray beam, are $P_1 = P_2$ (helicity) $= 0$, $P_3 = +1$, whereas the π and π' are linear components of x-rays parallel to the scattering plane for the incident and diffracted beam, respectively, and their stoke parameters are $P_1 = P_2 = 0$, $P_3 = -1$. Here $\sigma(\sigma')$, $\pi(\pi')$, and $\mathbf{k}_i(\mathbf{k}_f)$ has a right-handed relation ($\hat{\boldsymbol{\sigma}} \times \hat{\boldsymbol{\pi}} = \hat{\mathbf{k}}_i$ and $\hat{\boldsymbol{\sigma}}' \times \hat{\boldsymbol{\pi}}' = \hat{\mathbf{k}}_f$) as the x, y, and z axes has a right-handed coordinate system $\hat{x} \times \hat{y} = \hat{z}$. Each hat denotes the unit vector. The positive and negative circularly polarized x-rays are expressed by helicity $P_2 = +1$ and $P_2 = -1$, respectively. The positive (negative) circularly polarized x-rays are expressed by a sum of σ and π linear polarization in which the σ component is advanced (behind) in time by a phase $\frac{\pi}{2}$ to the π component and the spatial trace of the electric field of the positive (negative) circularly polarized x-rays at a point in time is a *left* (*right*)-handed screw, respectively. The azimuthal angle Ψ is a rotation of the sample about the scattering vector $\mathbf{k} = \mathbf{k}_f - \mathbf{k}_i$; opposite sign to [14] and the positive direction is clockwise as viewed looking up along the scattering vector $\mathbf{k}$. Here the origin of the azimuth angle $\Psi = 0$ is defined by the direction of the reciprocal lattice vector a^* axis when it is parallel to the y axis illustrated in the inset of figure 3.

We have successfully observed space group forbidden reflections 001 and 002 in the vicinity of the L_1 absorption edge. Figure 3 shows the intensity of forbidden reflection 001 observed as a function of energy E and azimuth angle Ψ in a range from $\Psi = -56.45$ to -69.2 with a 0.5° step. We find that reflection 001 is accompanied by strong multiple scattering effects which adds apparently random artefact to the spectra, which vary rapidly with Ψ. This well-understood effect can be seen in figures 4 and 5 as well. The underlying resonant reflection 001 at the L_1 edge is observed as a single peak (the

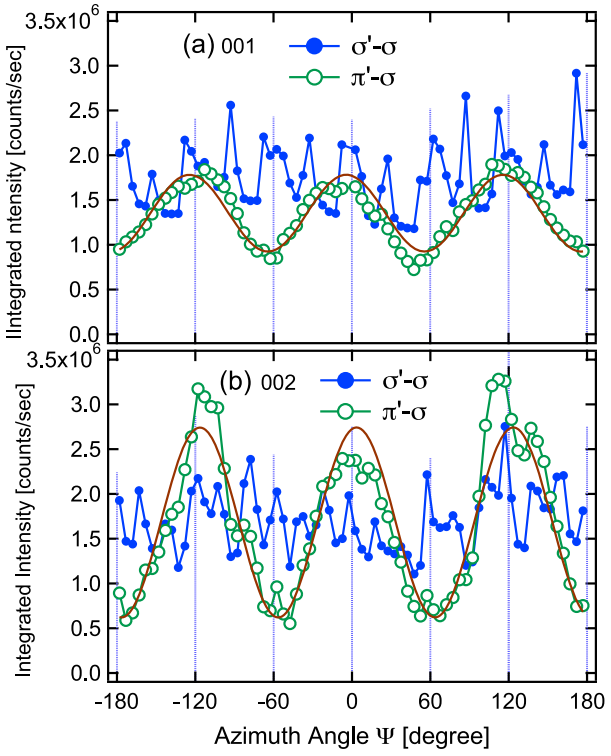

Figure 4. Integrated intensity of reflection 001 (panel (a)) and 002 (panel (b)) as a function of azimuthal angle Ψ observed with the incident beam at $E = 4.94$ keV. Closed and open circles represent the integrated intensity of the σ'–σ channel and π'–σ channel for the linearly polarized beam, respectively for reflection 001 and 002. Each cosine curve shows a result of fit to data with functions expressed by equation (2).

maximum is at $E = 4.94$ keV) with a shape (not the intensity) that is independent of azimuth angle Ψ.

2.2. Azimuthal angle scans

Resonant x-ray diffraction of space group forbidden reflections depends on the geometry of the scattering system as well as the energy of the x-ray beam. This is because resonant diffraction depends on the polarization state of the x-ray beam, and the unit-cell structure factor is described by a tensor. Hence the azimuth angle scan gives important information about the symmetry of the local structure of the resonant ions.

We have performed azimuthal angle scans for reflections 001 and 002 with and without a polarization analyser crystal, and with (σ) linear, and both positively and negatively circularly polarized incident beams, at an energy $E = 4.94$ keV. The integrated intensity of reflections 001 and 002 as a function of azimuthal angle Ψ for linearly polarized incident beam (σ) with a graphite analyser is shown in figure 4. The analyser 2θ angle $2\theta_a = 94°$ for reflection 004 of graphite gives an almost perfect polarization analysis ($\sin^2 2\theta_a = 0.995$). We find that each of the reflections 001 and 002 has a rather flat function for the σ'–σ channel while each has a cosine curve for the π'–σ channel. The 'noisy' structure for each azimuth scan curves is assumed to be due to the strong multiple scattering effect.

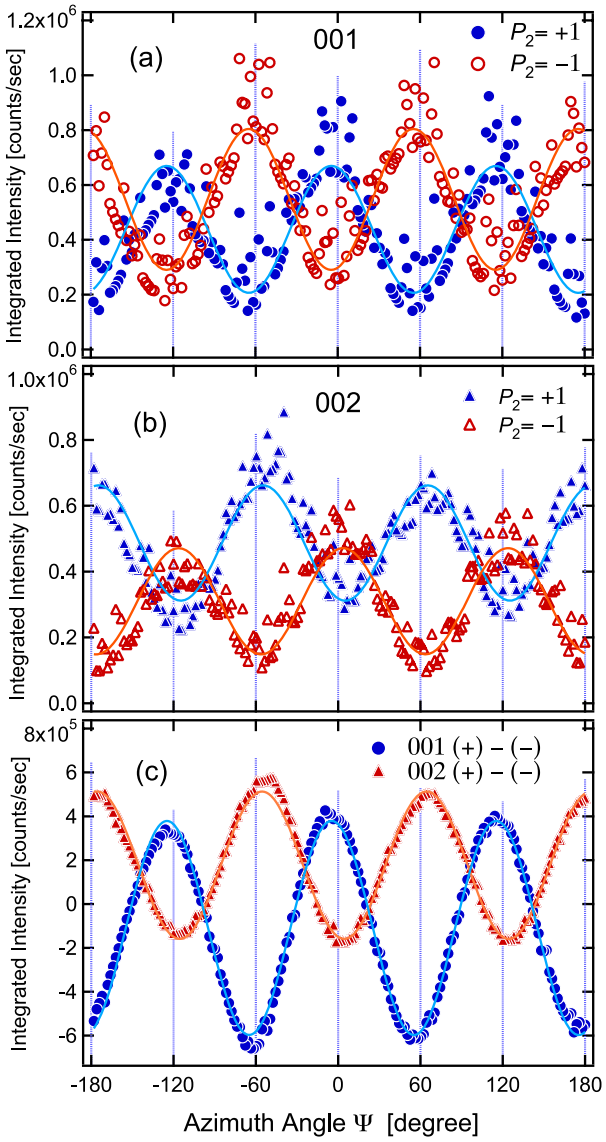

Figure 5. Integrated intensity of reflection 001 (a) and 002 (b) as a function of azimuthal angle Ψ, observed with the incident beam at $E = 4.94$ keV and a circularly polarized beam. Closed and open circles (triangles) represent the integrated intensity of the positive and the negative circularly polarized beam for reflection 001 (002), respectively. The difference intensity, $(+) - (-)$, between two polarizations of the incident beam for reflection 001 and 002 is shown in panel (c). Each cosine curve shows a result of a fit to data with functions expressed by equation (2).

The integrated intensity of reflections 001 and 002 as a function of azimuthal angle Ψ for circularly polarized incident beam, and the difference between opposite states of helicity, are shown in figure 5. The helicity of the incident beam, represented by $P_2 = \pm 1$, is switched with a diamond phase retarder. Taking the difference between the two helicity states eliminates the multi-scattering effect and gives smooth azimuthal functions for both reflections 001 and 002 as shown in panel (c). This is because multi-scattering is only very weakly dependent on the sign of circular polarization and cancels out by the subtraction.

Table 1. Inferred values of Y_0, A, and ψ of equation (2) obtained by a fit to the experimental data. Here $(+)-(-)$ shows the difference data between two helicity $(+)$ and $(-)$.

Reflection	Helicity	$Y_0 \times 10^5$	$A \times 10^5$	ψ (deg)
001	$P_2 = +1$	4.38 ± 0.72	2.31 ± 0.10	-4.66 ± 0.8
001	$P_2 = -1$	5.47 ± 0.74	-2.56 ± 0.10	-4.83 ± 0.8
001	$(+)-(-)$	-1.09 ± 0.02	4.88 ± 0.03	-4.75 ± 0.1
002	$P_2 = +1$	4.87 ± 0.49	-1.75 ± 0.07	5.29 ± 0.7
002	$P_2 = -1$	3.10 ± 0.44	1.61 ± 0.06	3.62 ± 0.7
002	$(+)-(-)$	1.77 ± 0.02	-3.36 ± 0.02	4.49 ± 0.1

To analyse the azimuth scan data collected for reflection $00l$, we adopt a function

$$I = Y_0 + A\cos\{3(\Psi - \psi)\} \tag{2}$$

to fit the azimuth scan data shown in figure 5, and summarize the parameters Y_0, A, and ψ in table 1. This function should have three-fold symmetry because of the crystal structure. Later we discuss the equation. The standard deviations of the fit to the data for the positive and negative helicity are quite large while those for the difference data shown in panel (c) are small.

From the difference intensity of azimuth angle scans for reflections 001 and 002, we find (i) that the 001 and 002 intensity difference data can be described by a symmetric cosine curve with a small phase shift of $\psi \sim \pm 4.5°$, (ii) the sign of which shift has an opposite sign for reflections 001 and 002 to each other, (iii) that the cosine curves of the difference intensity for reflection 001 and 002 are anti-phase to each other (the sign of parameter A is opposite to each other), and (iv) that the average of the cosine curve (parameter Y_0) for reflection 001 is negative while that for reflection 002 is positive. These experimental results enable us to determine the chirality of our Te sample absolutely.

3. Discussion

The intensity I of the resonant diffraction is described using the Stokes parameters $(0, P_2, P_3)$ as

$$\begin{aligned} I = {} & \tfrac{1}{2}(1 + P_3)(|G_{\sigma'\sigma}|^2 + |G_{\pi'\sigma}|^2) \\ & + \tfrac{1}{2}(1 - P_3)(|G_{\pi'\pi}|^2 + |G_{\sigma'\pi}|^2) \\ & + P_2\,\mathrm{Im}(G^*_{\sigma'\pi}G_{\sigma'\sigma} + G^*_{\pi'\pi}G_{\pi'\sigma}). \end{aligned} \tag{3}$$

Here $G_{\mu'\nu}$ is the total resonant scattering amplitude, and μ' and ν are the polarization state of the diffracted and incident x-ray beam, respectively. The third term represents the interference between σ and π components of the resonant scattering process for circularly polarized x-rays and plays a crucial role for determination of the chirality by changing the sign coupling with the helicity, P_2. This interference does not appear for conventional (Thomson) diffraction because there are no paths to change the polarization state, i.e. $G_{\pi'\sigma} = G_{\sigma'\pi} = 0$.

For multiple resonances we can write,

$$\begin{aligned} G_{\mu'\nu} &= \sum_k r^{(k)} \frac{F^{(k)}_{\mu'\nu}}{E - \Delta_k + \frac{\mathrm{i}}{2}\Gamma_k} \\ &= \sum_k d^{(k)}(E) F^{(k)}_{\mu'\nu}, \end{aligned} \tag{4}$$

where k represents individual resonant events, $E1E1$, $E1E2$ etc, Δ_k, Γ_k, and $r^{(k)}$ represent the resonant energy, its width, and the mixing parameter, respectively, and the scattering amplitude $F_{\mu'\nu}$ is

$$F_{\mu'\nu} = \sum_K X^{(K)}_{\mu'\nu} D^{(K)} \Psi^{(K)}. \tag{5}$$

In this expression, $\Psi^{(K)}$ represents the unit-cell structure factor spherical tensor of rank K ($K = 0$ (monopole), $K = 1$ (dipole), etc) which is the sum of atomic multipoles related to the resonant process, and $X^{(K)}_{\mu'\nu}$ describes conditions of the incident and the diffracted beam. Orientation of the crystal, with respect to states of polarization and the plane of scattering, is accomplished by a rotation matrix $D^{(K)}$. The theoretical description is described in detail in [9, 14].

The structure factor for the enantiomorphic space group pair #152 and #154 is fully described in [14]. Here we describe the structure factor and the intensity for circularly polarized x-rays briefly. As written in section 1, the difference between the two space groups is on the stacking sequence of atomic planes along the c axis. Te atoms locate at $(-x, -x, 0)$, $(x, 0, \pm\frac{1}{3})$, and $(x, 0, \mp\frac{1}{3})$ in a unit cell, respectively. Here the upper and lower sign of $\frac{1}{3}$ represent the space group #152 and #154, respectively. We keep this sign notation for the following discussion.

The most probable resonant process at the vicinity of the absorption edge L_1 of Te shown in figure 2 is the $E1E1$ event ($2s \leftrightarrow 5p$). Atomic multipoles related to the $E1E1$ event are $\langle T^{(K)}_Q \rangle$. Here rank $K = 2$ and the projection Q spans $-K \leqslant Q \leqslant K$. We take the ion at site $(-x, -x, 0)$ as a reference and describe the atomic multipole $\langle T^{(2)}_Q \rangle$ with a right-handed orthogonal quantization axes $(\xi\eta\zeta)$. Here ξ axis coincides with the diad axis of rotation symmetry through $(-x, -x, 0)$ and the ζ axis coincides with the crystal c axis. Note that our ξ axis lies in the plane spanned by reciprocal lattice vectors $\mathbf{a}^*$ (normal to direct vectors $\mathbf{b}$ and $\mathbf{c}$) and $\mathbf{b}^*$, with $\mathbf{a}^*$ and the ξ axis subtending an angle of 30°. Note, also, that the geometry for the experimental origin of $\Psi = 0$ is equivalent to the geometry when the ξ axis is parallel to the z axis due to the three-fold symmetry.

The unit-cell structure factor for #152 and #154, and reflection $00l$ ($l > 0$) is found to be

$$\Psi^{(2)}_Q = \langle T^{(2)}_Q \rangle \{1 + \mathrm{e}^{2\pi\mathrm{i}Q/3}\mathrm{e}^{2\pi\mathrm{i}(\pm l/3)} + \mathrm{e}^{-2\pi\mathrm{i}Q/3}\mathrm{e}^{2\pi\mathrm{i}(\mp l/3)}\}. \tag{6}$$

Here we find, for $00l$ reflections, the selection rule $l + Q = 3n$ for space group #152 and $l - Q = 3n$ for space group #154, where n is an integer. Space group allowed reflections satisfy the condition $Q = 0$ and $l = 3n$. Note that equation (6) appears to suggest that reversing the sign of l is equivalent to reversing the sign of Q, and thus the helicity. However, it should be remembered that such a reversal also requires a transformation of the tensor $T^{(K)}_Q$. The resulting scattering amplitude does not respect the apparent connection between the sign of l and the helicity of the crystal.

Accordingly the structure factors for reflection 001 for space group #152 and space group #154 are represented by a sum of $3\langle T^{(2)}_{-1} \rangle$ and $3\langle T^{(2)}_{+2} \rangle$, and a sum of $3\langle T^{(2)}_{+1} \rangle$

and $3\langle T^{(2)}_{-2}\rangle$, respectively. It is interesting to note that the relation between the structure factor and the space group is interchanged for reflection 002. This is because the phase factor in the calculation of the structure factor for reflection 001 and reflection 002 is opposite to each other. Finally, the intensity of 001 for space groups #152 and #154 for the $E1E1$ resonant event is found to be

$$I = I_0 + I_1\cos(3\Psi), \tag{7}$$

$$I_0 = \cos^2\theta T^2_\beta + \frac{1+\sin^2\theta}{2}\{1+\sin^2\theta + P_3\cos^2\theta - 2\nu P_2\sin\theta\}T^2_{\rm a}, \tag{8}$$

$$I_1 = \{2P_3\sin\theta + \nu P_2\cos^2\theta\}\cos\theta T_{\rm a}T_\beta. \tag{9}$$

Here I_0 and I_1 is constant and cosine terms in the azimuth scan (Ψ), respectively, θ is the Bragg angle, $T_{\rm a} = \frac{3}{2}\langle T^{(2)}_{+2}\rangle'$, and $T_\beta = \frac{3}{2}\langle T^{(2)}_{+1}\rangle''$ are the atomic multipoles, (the single prime and the double prime represent the real and the imaginary parts of each atomic multipole, respectively). We introduce a parameter $\nu = \pm 1$ to label the chirality, of which sign depends on the Miller indices $00l$ as well. For 001 reflection $\nu = +1$ for space group #152 and $\nu = -1$ for space group #154 while for reflection 002 the sign is reversed. Note that the sign of the P_2 terms in equations (8) and (9) is opposite to those in the equations described in [14] because we changed the definition of the scattering vector $\mathbf{k} = \mathbf{k}_{\rm f} - \mathbf{k}_{\rm i}$.

Let us analyse the azimuth scans shown in figures 4 and 5 using equations (7)–(9). Here experimental parameters θ, P_2, P_3 are known: $\sin\theta = 0.212$ for reflection 001 and $\sin\theta = 0.423$ for reflection 002. For the circularly polarized beam, $P_2 = \pm 1$ and $P_3 \simeq 0$, to a good approximation, and for the linearly polarized beam $P_3 = +1$. Parameters $T_{\rm a}$, and T_β, and ν are unknown. From the equations (8) and (9), the difference between two helicity states $P_2 = \pm 1$ is given as

$$I_0(+) - I_0(-) = -2\nu\sin\theta(1+\sin^2\theta)T^2_{\rm a} \tag{10}$$

$$I_1(+) - I_1(-) = +2\nu\cos^3\theta T_{\rm a}T_\beta. \tag{11}$$

Moreover the intensity for the $\sigma'\sigma$ and $\pi'\sigma$ channels [14] are,

$$I_{\sigma'\sigma} = T^2_{\rm a} \tag{12}$$

$$I_{\pi'\sigma} = \cos^2\theta T^2_\beta + \sin^2\theta T^2_{\rm a} + \sin 2\theta T_{\rm a}T_\beta\cos(3\Psi). \tag{13}$$

First, we find that equations (12) and (13) explain the azimuth scan data for the linearly polarized incident beam shown in figure 4 quite well: the intensity for the $\sigma'\sigma$ channel is almost flat, while the intensity for the $\pi'\sigma$ channel shows a three-fold cosine curve. Second, we find that equation (7) explains the azimuth scan data for the circularly polarized incident beam shown in figure 5 except a small the phase shift ψ found in equation (2). Here $I_0(+)-I_0(-) \simeq Y_0(+)-Y_0(-)$ and $I_1(+)-I_1(-) \simeq A(+)-A(-)$ hold in an assumption that the phase shift ψ in equation (2) is negligible. We suppose that the small phase shift ψ is due to the parity-odd resonant events like $E1E2$ or $E1M1$ as discussed in [14]. In these events, polar multipoles $\langle U^{(K)}_Q\rangle$ are observable. This introduction changes the equation (7) to

$$I = I_0 + I_1\cos(3\Psi) + I_2\sin(3\Psi), \tag{14}$$

The explicit expressions are found in equations (6.1)–(6.10) in [14].

Turning back to figure 5 and table 1, we find that the sign of $Y_0(+)-Y_0(-)$ is negative for reflection 001 and positive for reflection 002 and that the sign of $A(+)-A(-)$ is positive for reflection 001 and negative for reflection 002. The former gives $\nu = +1$ and the latter gives $\nu T_{\rm a}T_\beta > 0$. The latter itself does not give the sign of ν, however, we find that $T_{\rm a}T_\beta > 0$ from the azimuth scans for the $\pi'\sigma$ channel of reflections 001 and 002 as shown in figure 4 using equation (13). Hence we deduce $\nu = +1$ from I_1 as well. These results show that our Te sample is R Te (space group $P3_121$ #152). Moreover we can deduce the information on the atomic multipoles $T_{\rm a} = \frac{3}{2}\langle T^{(2)}_{+2}\rangle'$, and $T_\beta = \frac{3}{2}\langle T^{(2)}_{+1}\rangle''$ from the numerical data in table 1. Reflections 001 and 002 give similar values of the ratio $\langle T^{(2)}_{+2}\rangle'/\langle T^{(2)}_{+1}\rangle''$ as 0.81 and 0.73, respectively.

Note if the incident beam does not have 100% circular polarization and includes some amount of linear polarization (P_3) which keeps constant by switching the helicity, then, we could use it to advantage. The sign of P_2 changes not only the sign of I_1, but also the absolute value due to the additional contribution of the linear polarization. Hence, we know the chirality parameter from I_1 without a polarization analysis. Actually, this method has been applied to determine the structural chirality of berlinite $AlPO_4$ [17].

4. Optical rotatory power

We have performed an experiment on the optical rotatory power measurement on the same Te sample as was used for the resonant x-ray diffraction experiment. The infrared Fourier transform spectrometer at BL43IR, SPring-8, was employed for this task.

A sample, 1.3 mm thick, was placed between two polarizers. The first one was used as a pass filter permitting linear polarized light only, and the second one was used to measure the rotation of the polarization. The angle of the second polarizer was changed in a range from 0 to $-150°$ by a $-30°$ step. The negative sign corresponds to the counterclockwise rotation. The transmittance spectra is shown in panel (a) of figure 6. The wavenumber 2600 $\rm cm^{-1}$ is the energy gap of tellurium.

The optical rotatory power is obtained by taking the positions of the local maxima in these spectra. As shown in panel (b) of figure 6, the sample shows clearly laevorotatory since it rotates the light to the counterclockwise (to the left) as seen by an observer looking through the crystal towards the light source. The optical rotatory power γ at the wavenumber $\tilde{\nu} = 2000$ $\rm cm^{-1}$ is 58 ± 3 ($° \ \rm mm^{-1}$). This value is similar to the value 61 ($° \ \rm mm^{-1}$) obtained by Brown *et al* [5] and slightly larger than the value 56.8 ($° \ \rm mm^{-1}$) obtained by Nomura [12].

Thus, we find that our Te sample which belongs to the space group $P3_121$ has the optical laevorotatory power. This relationship between the sense of the structural chirality and the sense of optical activity of Te agrees nicely with the result obtained by the polarized neutron diffraction [5].

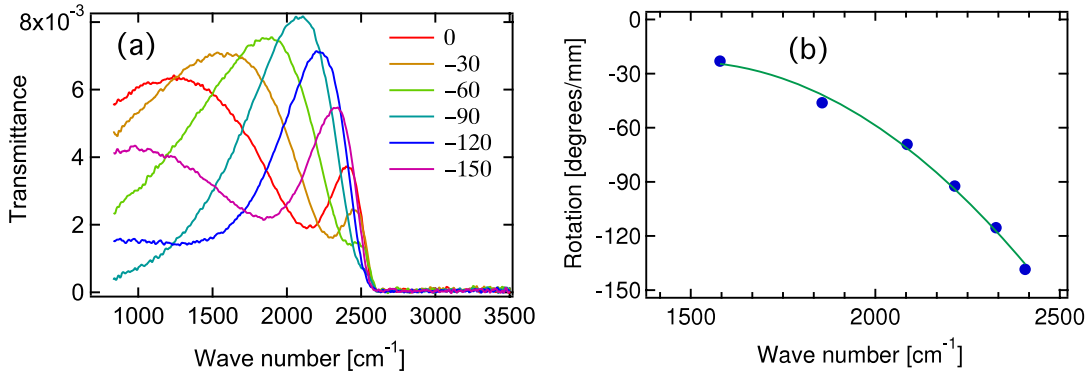

Figure 6. (a) Transmittance spectra for Te as a function of wavenumber for the angle of the second polarizer in a range from 0° to −150°. (b) The optical rotatory power. Rotation angle derived from panel (a) is normalized with the thickness.

5. Summary

We have performed a resonant x-ray diffraction experiment on a single crystal of tellurium which has an enantiomorphic space group pairs $P3_121$ and $P3_221$ with circularly polarized x-rays. We have observed the intensity of space group forbidden reflections 001 and 002 at the L_1 absorption edge of tellurium. By taking the difference intensity between two helicity of the circularly polarized x-ray beam, we have successfully determined the chirality of our tellurium sample as space group $P3_121$ unambiguously.

We also have performed an experiment on the optical rotatory power and found that our tellurium sample shows the optical laevorotatory power. This relationship between the sense of the structural chirality and the sense of optical activity of Te is consistent with the result obtained by the polarized neutron diffraction [5].

The advantage of our method is that the measurement of intensity of only one space group forbidden reflection is enough to determine the chirality. Thus, we have developed a new method to absolutely determine the crystal chirality (determination of one of an enantiomorphic space group pair). The technique is generally applicable to chiral motifs that occur in biomolecules, liquid crystals, ferroelectrics and antiferroelectrics, multiferroics, etc.

Acknowledgments

We thank Professor A M Glazer for valuable discussions about the optical rotatory power and the crystal structure. We are grateful to Dr Uschi Steigenberger who let us borrow her crystals of tellurium. One of us (SWL) is grateful to Dr K S Knight for on-going intellectual support. This work was partly supported by Grants-in-Aid for Scientific Research (A) No. 21244049 from JSPS.

References

[1] Bijvoet J M, Peerdeman A F and van Bommel A J 1951 *Nature* **168** 271
[2] Karle J 1980 *Int. J. Quantum Chem. Symp.* **7** 357
[3] Chandrasekaran K S 1968 *Acta Crystallogr.* A **24** 248
[4] McIntyre G J 1978 *Acta Crystallogr.* A **34** 936
[5] Brown P J and Forsyth J B 1996 *Acta Crystallogr.* A **52** 408
[6] Templeton D H and Templeton L K 1980 *Acta Crystallogr.* A **36** 237
[7] Templeton D H and Templeton L K 1982 *Acta Crystallogr.* A **38** 62
[8] Dmitrienko V E, Ishida K, Kirfel A and Ovchinnikova E N 2005 *Acta Crystallogr.* A **61** 481
[9] Lovesey S W *et al* 2005 *Phys. Rep.* **411** 233
[10] Cherin P and Unger P 1967 *Acta Crystallogr.* **23** 670
[11] Glazer A M and Stadnicka K 1986 *J. Appl. Crystallogr.* **19** 108
[12] Nomura K C 1960 *Phys. Rev. Lett.* **5** 500
[13] Tanaka Y *et al* 2008 *Phys. Rev. Lett.* **100** 145502
[14] Lovesey S W *et al* 2008 *J. Phys.: Condens. Matter* **20** 272201
[15] Landau L D and Lifshitz E M 1982 *Quantum Electrodynamics* 2nd edn, vol 4 (Oxford: Pergamon)
[16] Lovesey S W and Collins S P 1996 *X-Ray Scattering and Absorption by Magnetic Materials* (Oxford: Clarendon)
[17] Tanaka Y *et al* 2010 *Phys. Rev.* B submitted